



# Visualization of single-wall carbon nanotube (SWNT) networks in conductive polystyrene nanocomposites by charge contrast imaging

Joachim Loos<sup>a,b,c,\*</sup>, Alexander Alexeev<sup>a,d</sup>, Nadia Grossiord<sup>c,e</sup>,  
Cor E. Koning<sup>c,e</sup>, Oren Regev<sup>c,e,f</sup>

<sup>a</sup>Laboratory of Materials and Interface Chemistry, Eindhoven University of Technology, 5600 MB Eindhoven, The Netherlands

<sup>b</sup>Laboratory of Polymer Technology, Eindhoven University of Technology, 5600 MB Eindhoven, The Netherlands

<sup>c</sup>Dutch Polymer Institute, Eindhoven University of Technology, 5600 MB Eindhoven, The Netherlands

<sup>d</sup>NT-MDT Ltd., 124460, Moscow, Russia

<sup>e</sup>Laboratory of Polymer Chemistry, Eindhoven University of Technology, 5600 MB Eindhoven, The Netherlands

<sup>f</sup>Department of Chemical Engineering and The Ilse Katz Center for Meso and Nanoscale Science and Technology, Ben-Gurion University in the Negev, 84105 Beer-Sheva, Israel

Received 20 December 2004; received in revised form 7 March 2005; accepted 16 March 2005

## Abstract

The morphology of conductive nanocomposites consisting of low concentration of single-wall carbon nanotubes (SWNT) and polystyrene (PS) has been studied using atomic force microscopy (AFM), transmission electron microscopy (TEM) and, in particular, scanning electron microscopy (SEM). Application of charge contrast imaging in SEM allows visualization of the overall SWNT dispersion within the polymer matrix as well as the identification of individual or bundled SWNTs at high resolution. The contrast mechanism involved will be discussed. In conductive nanocomposites the SWNTs are homogeneously dispersed within the polymer matrix and form a network. Beside fairly straight SWNTs, strongly bended SWNTs have been observed. However, for samples with SWNT concentrations below the percolation threshold, the common overall charging behavior of an insulating material is observed preventing the detailed morphological investigation of the sample.

© 2005 Elsevier B.V. All rights reserved.

**Keywords:** Scanning electron microscopy (SEM); Charge contrast imaging; Single-wall carbon nanotubes; Conductive nanocomposites

\*Corresponding author. Department of Chemical Engineering and Chemistry, Eindhoven University of Technology, Den Dolech 2, 513 Eindhoven, The Netherlands.

Tel.: +0031 40 247 3033; fax: +0031 40 243 6999.

E-mail address: [j.loos@tue.nl](mailto:j.loos@tue.nl) (J. Loos).

## 1. Introduction

Recently discovered carbon nanotubes (CNT) [1], and especially single-wall nanotubes (SWNT),

offer fascinating properties: nanometric dimensions with a diameter of 1–3 nm and a high aspect ratio of about 1000, ultra-high structural integrity with an elastic modulus in the order of 1 TPa [2,3], and excellent 1D electric charge transport at room temperature [4,5]. The conductivity properties of SWNTs make them ideal wiring candidates for molecular-scale circuitry and devices, e.g., for applications in thin film field effect transistors (FETs) [6].

The unique combination of properties of the CNTs has also triggered the current interest in their use as filler material for polymer composites. It is reported that CNT/polymer composites show high strength and stiffness combined with electrical conductivity at relatively low concentrations of CNT [7–11]. Several CNT/polymer matrix systems have been studied in detail: nanotube-filled thermoplastic polymers such as polystyrene (PS) [12], poly(vinyl alcohol) [13], and polypropylene [14] as well as epoxy thermosets [15,16].

In a recent study of our research group, we have described a method to prepare SWNT-filled thermoplastic polymer nanocomposites based on latex technology [17]. We have shown that already at low concentrations of about 0.3 wt% SWNT the composites have indeed a conductivity of higher than  $10^{-2}$  S/m, which indicates that a conducting network of SWNTs exist in the polymer matrix. However, knowledge on the local organization of this network is very limited, but is imperative for understanding the physical mechanisms actually involved for charge transport, especially at such low SWNT concentrations.

Direct microscopic observation of the SWNT dispersion in nanocomposites is difficult to apply due to the extreme high aspect ratio of the SWNTs, the extreme difference in radial (1–3 nm) and axial dimensions ( $\sim 1 \mu\text{m}$ ). All common conventional microscopy techniques have their specific disadvantages concerning imaging the SWNT dispersion within a polymer matrix: optical microscopy only assesses very big agglomerates of nanotubes and is incapable to analyze the dispersion at the sub-micron scale [18–21]; surface-based methods, such as scanning electron microscopy (SEM) and scanning probe microscopy (SPM), or more specifically atomic force microscopy (AFM),

generally only show the surface or a cross-section of the three-dimensional arrangement of the SWNTs in the polymer matrix [21–23], and from transmission electron microscopy (TEM) images of thin sections (thickness  $\sim 100$  nm) it is difficult to draw conclusions on the bulk organization of the composite [24]. Moreover, identification of individual SWNTs in the polymer matrix by TEM is demanding because of low contrast between the SWNTs and the surrounding matrix.

It is the purpose of this study to show that conventional SEM is capable to provide (pseudo) three-dimensional morphological information on SWNT networks in conductive SWNT/PS nanocomposites at nanometric resolution by monitoring the sample in the charge contrast imaging mode. It is well known that insulating particles in a conductive matrix are charged up and shown as bright spots when examined under an intense electron beam in SEM [25]. The high negative potential developed in the insulating objects results in local differences of secondary electron emission, which enhances the contrast between the insulating particles and the conductive matrix. However, for a conductive filler in a dielectric matrix, such as a polymer, local charging and thus charge contrast formation is more complex and depends, e.g., upon the volume concentration and particle size distribution of the conductive fillers in the composite, but also on instrumental parameters of the SEM. Applications of charge contrast imaging dates back to 1983 [26]; however, so far only overall morphological investigations reaching rather low resolutions have been performed. It is our intention to demonstrate that SEM operated in charge contrast imaging mode is, to the best of our knowledge, virtually the only technique that is able to provide the required morphology information on the SWNT organization in the polymer matrix at several length scales, from nanometers to micrometers.

## 2. Experimental

To prepare nanocomposite samples, SWNTs from Carbolex Inc. (SWNT-AP <http://www.carbolex.com>) and sodium dodecylsulfate (SDS),

Aldrich) were used as received. PS was prepared through emulsion polymerization with SDS as surfactant and contains 30 wt% solids with an average diameter of 75 nm [27]. Solutions of 1:1 by weight of bare SWNTs and SDS in water were sonicated (Sonics vibracell VC750, 20 W, 20 kHz, 15 min) and centrifuged (Heraeus Sepatech Varifuge RF4655F equipped with a Sepatech rotor of 11 cm diameter, 4000 rpm for 30 min). The upper phase was taken and mixed with aqueous latex solution. The resulting mixture was freeze-dried (Christ Alpha 2–4 operated at 0.25 mbar and  $-80^{\circ}\text{C}$  overnight) prior to compression molding at  $180^{\circ}\text{C}$ , between poly(ethyleneterephthalate) sheets, using a Collin 300G hot press [17].

Morphological investigation of the as-prepared nanocomposites was performed using various microscopy techniques. To gain information on the nanometer-scale organization of the SWNT network in the nanocomposites, AFM, TEM and SEM were applied.

The AFM (Smena P47 H, NT-MDT, Moscow, Russia) was operated in intermittent contact mode in air using silicon cantilevers with spring constant  $k = 11\text{--}15\text{ N/m}$ , which were coated with a gold layer for higher laser beam reflectivity. Typical resonance frequencies were 210–230 kHz. The AFM was calibrated using a 25 nm height standard grating produced by NT-MDT Ltd.

TEM imaging of cross-sectional cut samples was performed. The as-prepared nanocomposite samples were sectioned at room temperature using an ultra-microtom (Reichert-Jung Ultracut E). The TEM (Jeol 2000FX) was operated in bright-field mode at 80 kV to increase the contrast between SWNTs and the surrounding polymer matrix.

The SEM (XL30 ESEM-FEG, Fei Co., Eindhoven, The Netherlands) was equipped with a field emission electron source. High vacuum conditions were applied and a secondary electron detector was used for image acquisition. The SEM was operated either in conventional high-voltage or low-voltage mode. No additional sample treatment such as surface etching or coating with a conductive layer had been applied. Standard acquisition conditions for charge contrast imaging were as follows: working distance of  $\sim 5\text{ mm}$  for low-voltage mode and  $\sim 10\text{ mm}$  for high-voltage

charge contrast imaging, spot 3, slow scan imaging with approximately 2 min/frame.

### 3. Results

Fig. 1 shows AFM height (Fig. 1a) and phase (Fig. 1b) contrast images, and a corresponding topography line scan (Fig. 1c) of the surface of an as-prepared SWNT/PS nanocomposite (SWNT concentration of 1.6 wt%). Large bright areas in both the height and phase images indicate the presence of hard metallic catalyst particles initially used to grow the SWNTs. Moreover, from both height and phase contrast images, line-like features with lengths of several hundreds of nanometers and much smaller width can be identified. These lines represent (parts of) individual or bundled SWNTs, which occasionally stick out or lie at the surface of the polymer film. In the central part of the images, the appearance of a valley-like depression suggests that a SWNT has been pulled off of the surface during sample preparation. The width of the SWNTs seems to be tens of nanometers. However, this is an artifact attributed to the specific curved shape of the AFM tip and the tip–SWNT interaction, and can be corrected by a deconvolution process [28]. Besides deconvolution, the authentic diameter of the SWNT can be determined by an accurate height measurement of a SWNT located at the surface of the sample and is in the order of 2 nm as shown in the topography line scan of Fig. 1c. However, still the presence of SWNT bundles cannot be excluded.

Further studies on the organization of SWNT/PS nanocomposites (1.6 wt% SWNT) were performed by TEM imaging of cross-sectional cut samples. Only occasionally, and mainly close to holes in the samples, we were able to image SWNTs covered with or sticking out of the polymer matrix (Fig. 2). Within the polymer matrix it is very difficult to visualize SWNTs because of lack of contrast. The TEM image confirms that the diameter of the exfoliated SWNTs used in our study is in the order of 2 nm (Fig. 2, SWNT marked by an arrow). Similar to AFM, TEM is able to visualize *individual* SWNTs with nanometer resolution. Unfortunately, based

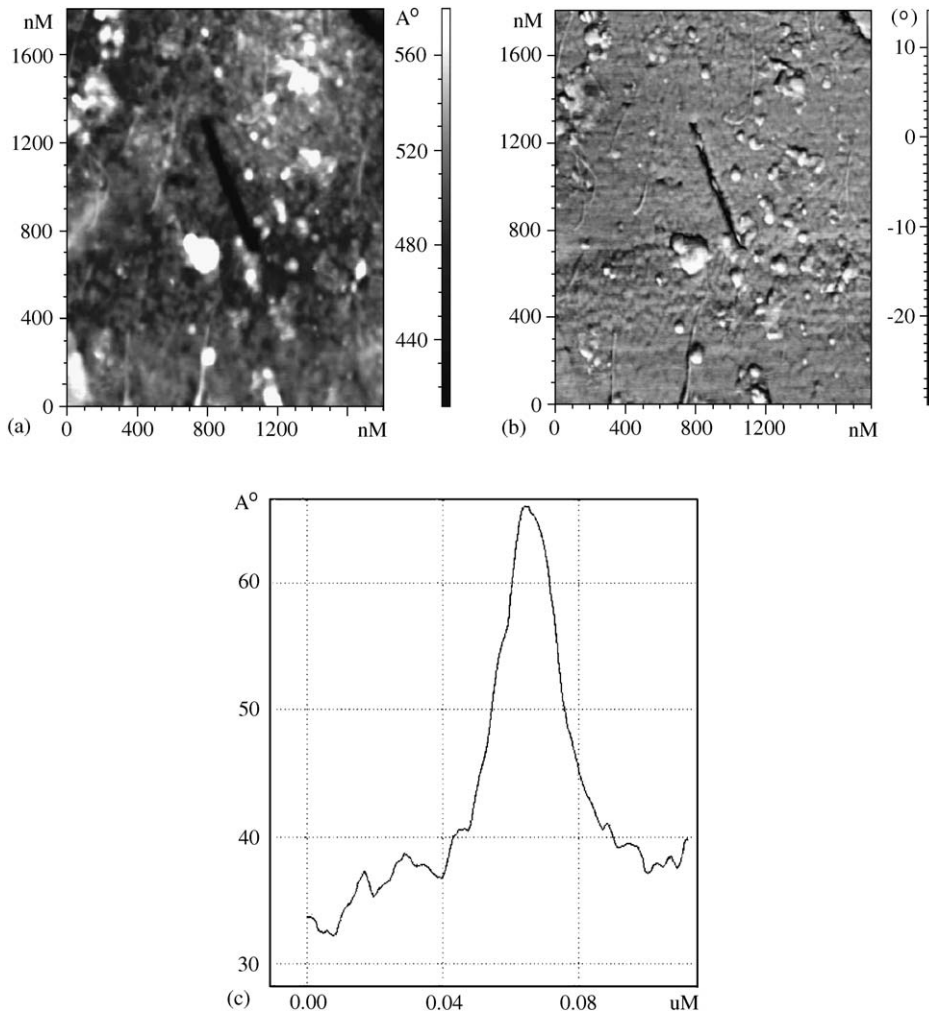


Fig. 1. Atomic force microscope (AFM) images of the surface of a SWNT/PS nanocomposite having a SWNT concentration of 1.6wt%; (a) height contrast, (b) phase contrast, and (c) corresponding topography line scan across a SWNT.

on the results obtained by AFM and TEM, it is difficult to draw conclusions about the homogeneity of the SWNT distribution in the polymer matrix, and—even more important for the present study—on the global organization of the conductive SWNT network.

Fig. 3 shows a series of high-resolution SEM images of the same region of a SWNT/PS nanocomposite (1.6 wt% SWNT) investigated at different acceleration voltages. For a low acceleration voltage of 1 kV, the primary electrons are able to penetrate the sample, which consists mainly

of carbon, in the order of few tens of nanometers. Thus, merely the surface of the sample can be investigated (Fig. 3a). No specific morphological features related to the presence of the SWNTs can be distinguished; some distinct (dust) particles (indicated by white arrows) and a horizontal scratch-like feature at the top of the image will be further used as landmarks to identify specific areas of the sample.

At an acceleration voltage of 5 kV, the overall appearance of the same sample area has changed (Fig. 3b). Still the two particles and the horizontal

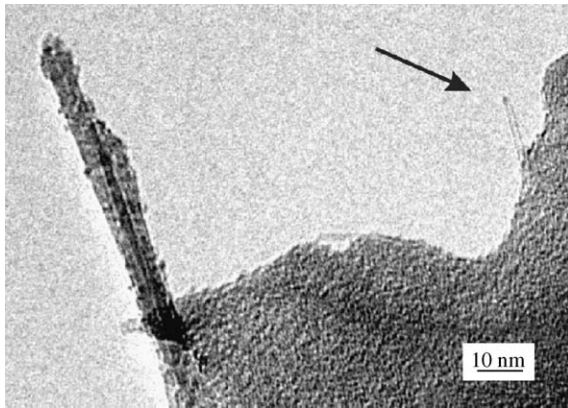


Fig. 2. Bright-field TEM image of a cross section of a SWNT/PS nanocomposite sample (1.6wt% of SWNT) showing SWNTs covered with PS matrix (left side of the image) and a SWNT sticking out of the PS matrix (marked by an arrow).

scratch can be recognized. However, the relative brightness of the particles has increased, which might be an indication for local charging. Moreover, everywhere but especially in the central region of the image some bright lines can be observed, which have a length in the order of 1  $\mu\text{m}$  and a width of  $\sim 30$  nm. These lines represent individual or bundled SWNTs.

Because of the different capabilities for charge transport of the conductive SWNT and the insulating polymer matrix, the secondary electron yield is enriched at the location of the SWNT, which results in the contrast between the SWNT network and the polymer matrix. However, from a theoretical point of view, the contrast should be inverted, as discussed in the Introduction; the SWNTs should appear dark in a bright since charged polymer matrix. This contrast mechanism is not applicable for the low acceleration voltage of 1 kV, where charging is prevented (Fig. 3a). Local charging of the polymer matrix around the SWNTs may have rendered the average diameter of the SWNTs to be one order of magnitude larger than the value measured for an individual SWNT by AFM or TEM. Recently, a similar contrast enhancement and rendering of the diameter of SWNTs deposited on a silicon substrate has been reported [29].

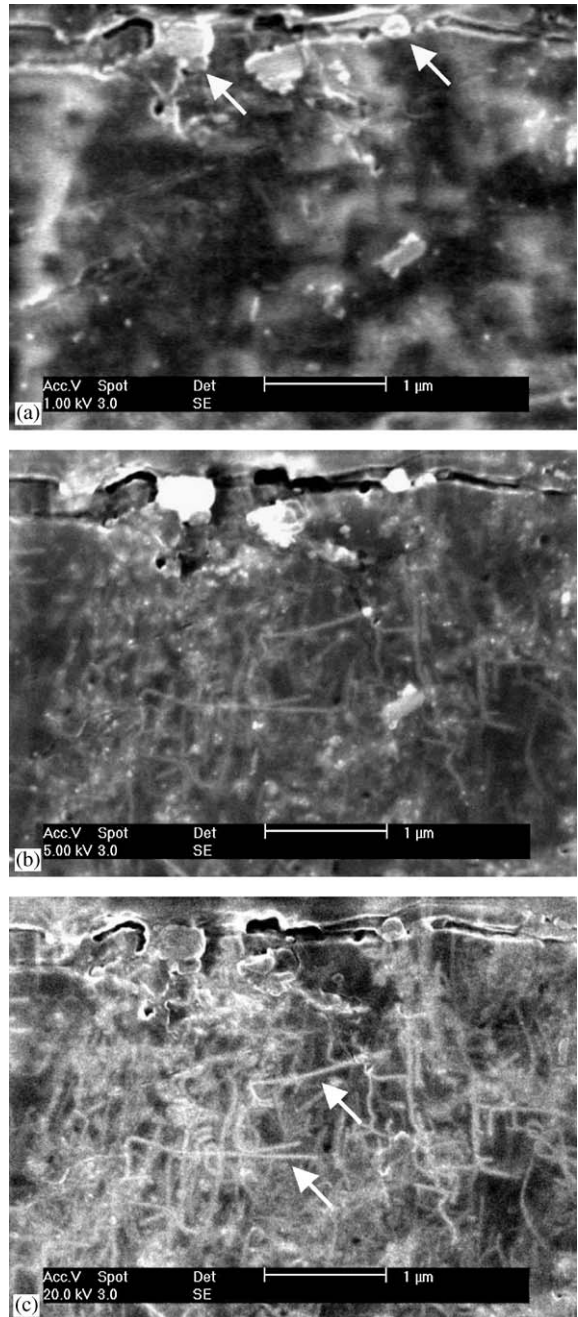


Fig. 3. Series of high-resolution SEM images of the same region of a SWNT/PS nanocomposite having a SWNT concentration of 1.6wt%, using an acceleration voltage of (a) 1, (b) 5, and (c) 20 kV. The arrows in (a) indicate reference particles, the arrows in (c) indicate SWNTs also visible in Fig. 3b.

In Fig. 3c, acquired at an acceleration voltage of 20 kV, again the horizontal scratch and the two particles used as landmarks can be identified. Moreover, a large number of bright lines can be seen, which again represent SWNTs. In contrast to Fig. 3b, the number of SWNTs is much higher and a network-like morphology emerges. The rather straight nanotubes aligned horizontally in the central area of the image (marked by arrows) were already vaguely visible in Fig. 3b.

But why does the number of visible SWNTs in the polymer matrix increases hand in hand with increased acceleration voltage? At this moment, it is not fully clear to us whether we simply observe further contrast enhancement of SWNTs near to or at the surface of the specimen, or whether we are able to gain additional morphological information on the SWNT organization inside the sample when applying high primary electron energies for the investigation. At an acceleration voltage of 20 kV, the penetration depth of the primary electrons is in the order of 2  $\mu\text{m}$  for a carbon sample [30]. This may correspond with an increased information depth in Fig. 3c when compared with Figs. 3a and 3b, acquired at lower acceleration voltages.

The actual penetration depth of primary electrons in a sample depends on the acceleration voltage applied. This can be demonstrated by using either the Kanaya–Okayama range calculations or Monte Carlo simulation routines. The Kanaya–Okayama range is given by

$$R_{\text{KO}} = 2.76 \times 10^{-11} A E_0^{1.67} / (Z^{0.889} \times d) \text{ cm}, \quad (1)$$

where  $E_0$  is the incident electron energy in keV,  $A$  is the average atomic weight in g,  $d$  is the density of the material in  $\text{g}/\text{cm}^3$ , and  $Z$  is the atomic number of the target [31].

Analyzing always the same area of the nanocomposite sample, with increased acceleration voltage the penetration depth of the electrons increases, and thus the actual sample volume probed becomes larger. Consequently, for SWNTs homogeneously distributed in a polymer matrix, the number of visible SWNTs will rise with increasing acceleration voltage used. The sketch of Fig. 4 elucidates this behavior: for a low acceleration voltage, only some SWNTs near to

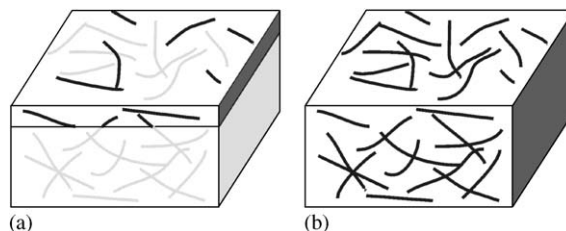


Fig. 4. Representation of the sample depth/volume probed with (a) low and (b) high acceleration voltages; the black lines represent SWNTs visible for the acceleration voltage used, gray lines in (a) represent SWNTs not visible for low acceleration voltage.

or at the surface of the specimen are seen (dark lines in Fig. 4a), but for high acceleration voltages, these SWNTs and additional SWNTs being positioned deeper in the sample are detected (Fig. 4b).

Moreover, comparing the number of nanotubes visible using AFM or SEM at low acceleration voltages is similar for same SWNT concentration in the sample, whereas the number of nanotubes detected at high acceleration voltages is substantially larger. This observation supports that using charge contrast imaging at high acceleration voltage, we are able to gain representative information on the three-dimensional organization of a conductive single-wall CNT network in a polymer matrix. The SEM charge contrast images represent a two-dimensional visualization of these three-dimensional SWNT network structures in the polymer matrix. The brightness variations visible in the SEM charge contrast images can be related to the position of the SWNTs in the sample: high brightness means a position of the SWNTs at or near to the surface, whereas SWNTs located deep in the nanocomposite appear darker. However, also other explanations for the brightness variations of the SWNTs might be possible. E.g. it cannot be excluded that parts of the SWNT network are disconnected from the major part of the network (disconnected from ground, lower brightness), but the presence of a mixture of conductive (high brightness) and semi-conductive (low brightness) nanotubes [32] is a possibility as well.

Applying charge contrast imaging to the conductive SWNT/PS nanocomposites, more insight

in the local organization of the SWNTs has been obtained. Having an elastic modulus in the order of 1 TPa [2,3], SWNTs are the stiffest synthetic materials; however, they have the ability to bend. Embedded in polymer matrixes, somewhat curved CNTs have been monitored using TEM or AFM [17,33,34]. Fig. 5a shows an overview charge contrast image of a SWNT/PS nanocomposite obtained at an acceleration voltage of 20 kV. A substantial amount of CNTs is homogeneously distributed over the entire area of the image. Details on the local organization of *individual* SWNTs can be seen in Fig. 5b. The sample

observed has a SWNT concentration of 0.3 wt%. Besides fairly straight SWNTs, a large number of SWNTs are curved. Some of the SWNTs are bended so much that they form circular structures with a diameter below 100 nm. Such strong bending behavior demonstrates the supreme flexibility of the SWNTs and has been imaged previously only for SWNTs suspended in solution [35].

In contrast to samples having a SWNT concentration above the percolation threshold for the formation of a conductive network, samples with SWNT concentrations below the percolation threshold show strong charging at high acceleration voltages, which prevents imaging of details of the SWNT organization in the polymer matrix: only overall charging of the sample is observed, which is comparable to the results obtained by Chung et al. on other insulating systems [26].

#### 4. Conclusions

We have investigated the morphology of conductive single-wall CNT networks embedded in PS matrices. Using low voltage and conventional SEM, operated in the charge contrast imaging mode, individual or bundled SWNTs and the overall organization of the conductive SWNT network can be visualized. With increasing acceleration voltage, the secondary electron yield at the positions of the SWNTs increases and enhances the contrast between SWNTs and the matrix. However, local charging of the polymer matrix around the SWNTs may have rendered the average diameter of the SWNTs to be  $\sim 30$  nm, which is one order of magnitude above the value of the diameter for SWNTs as measured by AFM or TEM.

For a given sample area, we find that the number of visible SWNTs in the polymer matrix increases with increased energy of the primary electron beam. This behavior can be explained with an increased sample volume probed, because the penetration depth of the primary electrons increases with increasing acceleration voltage, and is, e.g., in the order of  $2\ \mu\text{m}$  for an acceleration voltage of 20 kV for samples composed mainly of

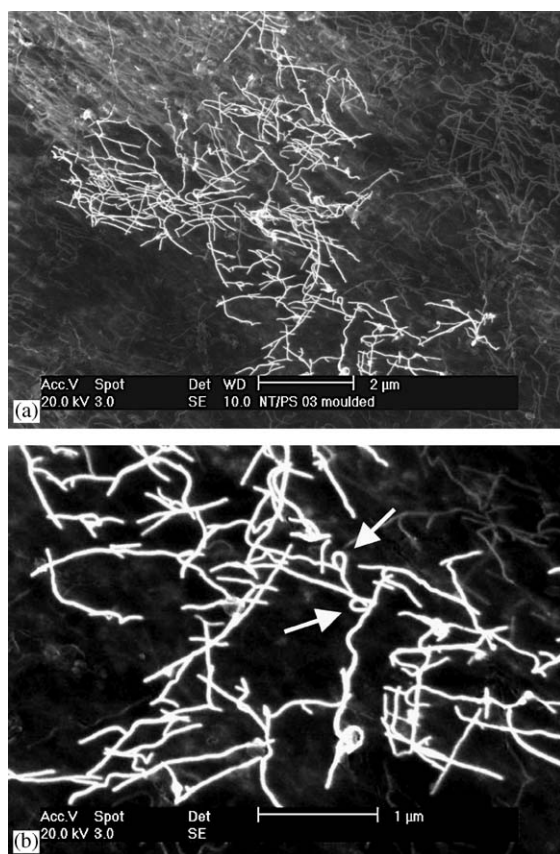


Fig. 5. (a) Overview and (b) high-resolution SEM charge contrast image acquired at an acceleration voltage of 20 kV showing fairly straight and bended SWNTs. The SWNT concentration is 0.3 wt%. Attention should be paid to strongly curved SWNTs (marked by arrows), and to the different brightness of the SWNTs.

carbon. Using charge contrast imaging of the SWNT network at such high acceleration voltages, quasi-three-dimensional information on the organization of the conductive SWNT network can be obtained. Quantification of this information to, e.g., recalculate the SWNT concentration in the nanocomposite is the objective of ongoing research. In addition, from the charge contrast images details on the local organization of the SWNTs can be analyzed. Both, fairly straight as well as strongly bended SWNTs have been observed.

### Acknowledgments

The authors are thankful for the support of the Dutch Polymer Institute (DPI), project 416. We are very grateful to Paul van der Schoot for helpful discussions. Michel Peppers and Paul de Boer are kindly acknowledged for their assistance.

### References

- [1] S. Iijima, *Nature* 354 (1991) 56.
- [2] M.-F. Yu, B.S. Files, S. Arepalli, R.S. Ruoff, *Phys. Rev. Lett.* 84 (2000) 5552.
- [3] E. Dujardin, T.W. Ebbesen, A. Krishnan, P.N. Yianilos, M.M.J. Treacy, *Phys. Rev. B* 58 (1998) 14013.
- [4] S. Frank, P. Poncharal, Z.L. Wang, W.A. de Heer, *Science* 280 (1998) 1744.
- [5] J.N. Coleman, S. Curran, A.B. Dalton, A.P. Davey, B. McCarthy, W. Blau, R.C. Barklie, *Phys. Rev. B* 58 (1998) R7492.
- [6] E.S. Snow, J.P. Novak, P.M. Campbell, D. Park, *Appl. Phys. Lett.* 82 (2003) 2145.
- [7] J.H. Rouse, P.T. Lillehei, *Nanoletters* 3 (2003) 59.
- [8] Z. Jin, K.P. Pramoda, G. Xu, S.H. Goh, *Chem. Phys. Lett.* 337 (2001) 43.
- [9] D. Qian, E.C. Dickey, R. Andrews, T. Rantell, *Appl. Phys. Lett.* 76 (2000) 2868.
- [10] L.S. Schadler, S.C. Giannaris, P.M. Ajayan, *Appl. Phys. Lett.* 73 (1998) 3842.
- [11] M.J. Biercuk, M.C. Llaguno, M. Radosavljevic, J.K. Hyun, A.T. Johnson, J.E. Fischer, *Appl. Phys. Lett.* 80 (2002) 2767.
- [12] A. Dufresne, M. Paillet, J.L. Putaux, R. Canet, F. Carmona, P. Delhaes, *J. Mater. Sci.* 37 (2002) 3915.
- [13] M.S.P. Shaffer, A.H. Windle, *Adv. Mater.* 11 (1999) 937.
- [14] L. Valentini, J. Biagotti, J.M. Kenny, S. Santucci, *J. Appl. Polym. Sci.* 87 (2003) 708.
- [15] X.G. Gong, J. Liu, S. Baskaran, R.D. Voise, J.S. Young, *Chem. Mater.* 12 (2000) 1049.
- [16] J. Sandler, M.S.P. Shaffer, T. Prasse, W. Bauhofer, K. Schulte, A.H. Windle, *Polymer* 40 (1999) 5967.
- [17] O. Regev, P.N.B. El Kati, J. Loos, C.E. Koning, *Adv. Mater.* 16 (2004) 248.
- [18] R. Andrews, D. Jacques, M. Minot, T. Rantell, *Macromol. Mater. Eng.* 287 (2002) 395.
- [19] A.R. Bhattacharyya, T.V. Sreekumar, T. Liu, S. Kumar, L.M. Ericson, R.H. Hauge, R.E. Smalley, *Polymer* 44 (2003) 2373.
- [20] H.J. Barraza, F. Pompeo, E.A. O'Rear, D.E. Resasco, *Nanoletters* 2 (2002) 797.
- [21] B. Safadi, R. Andrews, E.A. Grulke, *J. Appl. Polym. Sci.* 84 (2002) 2660.
- [22] C.A. Cooper, D. Ravich, D. Lips, J. Mayer, H.D. Wagner, *Compos. Sci. Technol.* 62 (2002) 1105.
- [23] Z. Roslaniec, G. Broza, K. Schulte, *Compos. Interface* 10 (2003) 95.
- [24] M. Sennett, E. Welsh, J.B. Wright, W.Z. Li, J.G. Wen, Z.F. Ren, *Appl. Phys. A* 76 (2003) 111.
- [25] O.C. Wells, *Scanning Electron Microscopy*, McGraw-Hill, New York, 1974.
- [26] K.T. Chung, J.H. Reisner, E.R. Campbell, *J. Appl. Phys.* 54 (1983) 6099.
- [27] R.G. Gilbert, *Emulsion Polymerization: A Mechanistic Approach*, Academic Press, London, 1995.
- [28] D.J. Keller, F.S. Franke, *Surf. Sci.* 294 (1993) 409.
- [29] M.R. Diehl, S.N. Yaliraki, R.A. Beckman, M. Barahona, J.R. Heath, *Angew. Chem. Int. Ed.* 41 (2002) 353.
- [30] M.P. Seah, W.A. Dench, *Surf. Interface Anal.* 1 (1979) 2.
- [31] K. Kanaya, S. Okayama, *J. Phys. D* 5 (1972) 43.
- [32] M. Ouyang, J.-L. Huang, C.L. Cheung, C.M. Lieber, *Science* 292 (2001) 702.
- [33] C. Bower, R. Rosen, L. Jin, J. Han, O. Zhou, *Appl. Phys. Lett.* 74 (1999) 3317.
- [34] P. Pötschke, A.R. Bhattacharyya, A. Janke, *Eur. Polym. J.* 40 (2004) 137.
- [35] V.C. Moore, M.S. Strano, E.H. Haroz, R.H. Hauge, R.E. Smalley, J. Schmidt, Y. Talmon, *Nanoletters* 3 (2003) 1379.